Forbidden Backscattering and Resistance Dip in the Quantum Limit as a Signature for Topological Insulators

Yiyuan Chen,[1,2] Hai-Zhou Lu,[1,2,*] and X. C. Xie[3,4]

[1]*Shenzhen Institute for Quantum Science and Technology and Department of Physics, Southern University of Science and Technology, Shenzhen 518055, China*

[2]*Shenzhen Key Laboratory of Quantum Science and Engineering, Shenzhen 518055, China*

[3]*International Center for Quantum Materials, School of Physics, Peking University, Beijing 100871, China*

[4]*Collaborative Innovation Center of Quantum Matter, Beijing 100871, China*

(Received 2 February 2018; revised manuscript received 2 May 2018; published 20 July 2018)

Identifying topological insulators and semimetals often focuses on their surface states, using spectroscopic methods such as angle-resolved photoemission spectroscopy or scanning tunneling microscopy. In contrast, studying the topological properties of topological insulators from their bulk-state transport is more accessible in most labs but seldom addressed. We show that, in the quantum limit of a topological insulator, the backscattering between the only two states on the Fermi surface of the lowest Landau band can be forbidden at a critical magnetic field. The conductivity is determined solely by the backscattering between the two states, leading to a resistance dip that may serve as a signature for topological insulator phases. More importantly, this forbidden backscattering mechanism for the resistance dip is irrelevant to details of disorder scattering. Our theory can be applied to revisit the experiments on $Pb_{1-x}Sn_xSe$, $ZrTe_5$, and Ag_2Te families, and will be particularly useful for controversial small-gap materials at the boundary between topological and normal insulators.

DOI: 10.1103/PhysRevLett.121.036602

Introduction.—Three-dimensional topological insulators [1–3] are characterized by topologically protected 2D surface states. Most works focus on the surfaces, because they are also outposts for more exotic topological phases [4–7] that are of potential application in next-generation electronic devices. However, in most samples, the bulk electrons overwhelm the surface electrons as the major carriers in the transport. Identifying topological insulators by detecting the bulk-state transport is an appealing topic of fundamental interest.

In a strong magnetic field, the 3D bulk states of a topological insulator quantize into 1D Landau bands. The lowest Landau band may inherit the topological information. In 2D, the crossing of the lowest Landau levels (not bands) has been used as a signature for the quantum spin Hall phase [8,9]. But in 3D, how the lowest Landau band can be used to distinguish a topological insulator is seldom addressed. In this work, we study the resistance of a 3D topological insulator in parallel magnetic fields and when only the lowest Landau band is occupied, i.e., in the quantum limit [Fig. 1(b)]. We find that for topological insulator phases, the backscattering in the quantum limit can be completely suppressed at a critical magnetic field. This suppression is irrelevant to the nature of the impurity scattering, and only depends on the spinor eigenstate of the lowest Landau band. As the backscattering is forbidden, the transport time diverges, and the resistivity shows a dip. This resistance dip resulting from the forbidden backscattering is absent in the trivial insulator phase, and thus can be used as a signature for the topological insulator phases. The mechanism of the forbidden backscattering is an eigenstate property and thus is new and different from the mechanism of Landau level crossing, which is a spectrum property. Also, this forbidden backscattering is absent in topological semimetals [10–12]. Our theory is in good agreement with a recent experiment [Figs. 1(c) and 1(d)] and can be very useful for controversial small-gap materials at the boundary between topological insulators and normal insulators.

Model and the quantum limit.—We start with a well-accepted $k \cdot p$ Hamiltonian for the bulk states in a topological insulator [3,19,20]:

$$H_0 = C_{\boldsymbol{k}} + \begin{bmatrix} M_{\boldsymbol{k}} & 0 & iV_n k_z & -iV_\perp k_- \\ 0 & M_{\boldsymbol{k}} & iV_\perp k_+ & iV_n k_z \\ -iV_n k_z & -iV_\perp k_- & -M_{\boldsymbol{k}} & 0 \\ iV_\perp k_+ & -iV_n k_z & 0 & -M_{\boldsymbol{k}} \end{bmatrix}, \quad (1)$$

where $M_{\boldsymbol{k}} = M_0 + M_\perp(k_x^2 + k_y^2) + M_z k_z^2$, $C_{\boldsymbol{k}} = C_0 + C_\perp(k_x^2 + k_y^2) + C_z k_z^2$, and k_x, k_y, k_z are the wave vectors, M_i, V_i, and C_i are model parameters. With both $M_0 M_\perp < 0$ and $M_0 M_z < 0$, the model describes a 3D strong topological insulator with topologically protected surface states at all surfaces. Although a simple $k \cdot p$ model, it has been shown effective in the theories that work well for experiments, such as giving proper descriptions for the

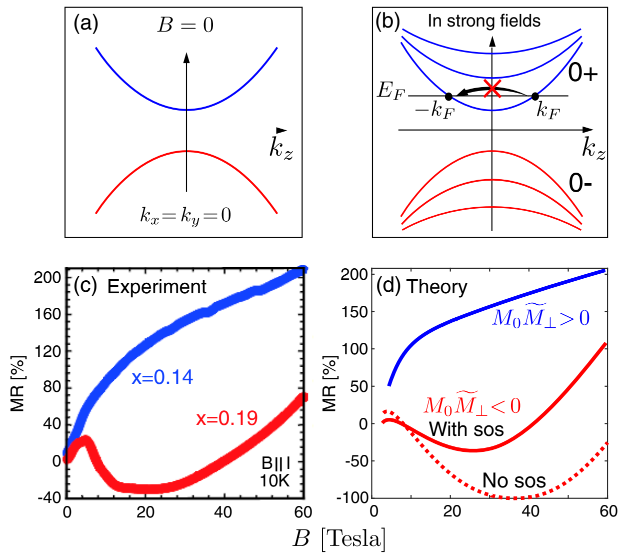

FIG. 1. In the quantum limit of a 3D topological insulator, the backscattering between the only two states at the Fermi energy can be forbidden at a critical magnetic field, leading to a resistance dip. (a) The zero-field energy spectrum vs k_z of a 3D topological insulator at $k_x = k_y = 0$. (b) In a strong magnetic field, the lowest Landau energy bands of the 3D topological insulator vs k_z. The Fermi energy E_F crosses only the 0+ Landau band. k_F and $-k_F$ stand for the only two states at the Fermi energy. (c) The magnetoresistance of $Pb_{1-x}Sn_xSe$ adapted from Ref. [13]. (d) The calculated magnetoresistance using Eq. (14) (see Sec. S2B of Ref. [14] for details). The abbreviation "sos" means spin-orbit scattering. The parameters are $M_0 = -0.01$ eV, $M_z = 0$, $\tilde{M}_\perp = 18$ eV Å^2, $\alpha_1 = 100$ eV T, and $\alpha_2 = 0.0025$ eV T^{-2}.

topological surface states [21–23] and explaining the negative magnetoresistance in topological insulators [24–28].

In a strong magnetic field B along the z direction, the energy spectrum quantizes into a series of 1D Landau bands [Figs. 1(a) and 1(b)]. The energies of the lowest two Landau bands, denoted as 0+ and 0−, are $E_{0\pm} = C_0 + C_z k_z^2 + C_\perp/\ell_B^2 \pm \sqrt{m^2 + V_n^2 k_z^2}$, where the magnetic length $\ell_B \equiv \sqrt{\hbar/eB}$, $-e$ is the electron charge, and the mass term

$$m = M_0 + M_z k_z^2 + M_\perp/\ell_B^2. \tag{2}$$

The gap between the lowest Landau bands can be determined by m with $k_z = 0$.

In the following, we will focus on an electron-doped quantum limit where the Fermi energy crosses only the 0+ Landau band, whose eigenstate is found to be

$$|0,+,k_x,k_z\rangle = \begin{bmatrix} 0 \\ -i\sin(\theta/2) \\ 0 \\ \cos(\theta/2) \end{bmatrix} |0,k_x,k_z\rangle, \tag{3}$$

where we have defined

$$\cos\theta \equiv \frac{-m}{\sqrt{m^2 + (V_n k_z)^2}}, \tag{4}$$

and $|0,k_x,k_z\rangle$ denotes the state of a usual zeroth Landau level timing a plane wave along the z direction [10].

Forbidden backscattering.—The electronic transport in solids is more or less affected by the backscattering. In particular, the backscattering plays a dictating role in the present 1D Landau band, because there are only two states at the Fermi energy, as indicated by k_F and $-k_F$ in Fig. 1. The backscattering between these two states is characterized by the scattering matrix element between them. Using the spinor eigenstate in Eq. (3), the modular square of the scattering matrix element between the k_F and $-k_F$ states is found to be proportional to the form factor

$$I_S = \cos^2\theta|_{k_z=k_F}. \tag{5}$$

I_S vanishes when $m = 0$, which means that the backscattering between state k_F and state $-k_F$ is forbidden. According to Eq. (2), m vanishes at a critical magnetic field B_c determined by $M_0 + M_z k_F^2 + M_\perp e B_c/\hbar = 0$, where k_z becomes the Fermi wave vector k_F at the Fermi energy. For a topological insulator, $M_0 M_z < 0$ and $M_0 M_\perp < 0$, so B_c has finite solutions at which the backscattering is completely suppressed. Later, we will show that this forbidden backscattering can lead to a dip in the resistance as a function of the magnetic field, which can be probed in experiments and can give a signature for topological insulator phases. We emphasize that this forbidden backscattering is an eigenstate property and thus is new and different from the mechanism of Landau level crossing [8,9], which is a spectrum property.

Zero point in form factor.—Now, we analyze the zero points of I_S, at which the backscattering is forbidden. For a fixed carrier density n, the Fermi wave vector k_F depends on B in terms of $k_F = 2\pi^2\hbar n/eB$ [10], so m becomes

$$m = M_0 + M_z\left(\frac{2\pi^2\hbar n}{e}\right)^2 \frac{1}{B^2} + M_\perp \frac{e}{\hbar} B. \tag{6}$$

Depending on the signs of M_0, M_z, $M_\perp$, we have three phases: (i) Strong topological insulator, $M_0 M_z < 0$ and $M_0 M_\perp < 0$. (ii) Weak topological insulator, $M_0 M_z < 0$ and $M_0 M_\perp \geq 0$, or $M_0 M_z \geq 0$ and $M_0 M_\perp < 0$. (iii) Trivial insulator, $M_0 M_z \geq 0$ and $M_0 M_z \geq 0$. Figure 2 shows m in Eq. (6) and the corresponding I_S as functions of B for the three phases. Every time m has a zero point, I_S also has a zero point. For the trivial insulator phase, I_S has no zero point. For both the weak and strong topological insulator phases, I_S has one zero point in the quantum limit. For a strong topological insulator, I_S may have two zero points (Fig. 2, row 1, column 3), in which case our theory may not

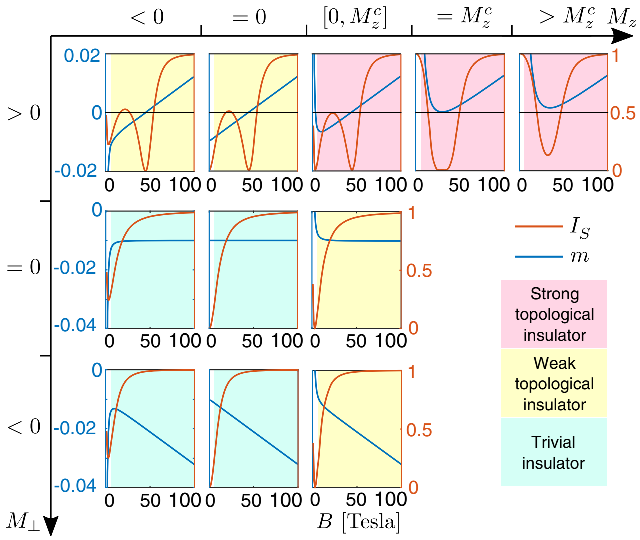

FIG. 2. The mass term m and form factor I_S as functions of the magnetic field B for $M_0 < 0$ and different $M_\perp$ and M_z. Red, yellow, and green backgrounds indicate the quantum limit for a carrier density of $6 \times 10^{16}/\mathrm{cm}^3$. Without loss of generality, we have assumed $M_0 < 0$, so $M_\perp > 0$ and $M_z > 0$ means a strong topological insulator, $M_\perp \leq 0$ and $M_z \leq 0$ means a trivial insulator, $M_\perp \leq 0$ and $M_z > 0$ means a weak topological insulator (001), and $M_\perp > 0$ and $M_z \leq 0$ means a weak topological insulator (110). The parameters are $M_0 = -0.01$ eV; $M_z = -27$, 0, 27, 820, 1200 eV Å^2 from left to right; and $M_\perp = -13.5$, 0, 13.5 eV Å^2 from bottom to top.

apply to the lower one, because it may not be within the quantum limit for realistic model parameters. In addition, above a critical value M_z^c, there is no zero point (Fig. 2, row 1, columns 4 and 5). But the corresponding M_z^c is too large (205 eV Å^2 for the material we discuss) to be regarded as reasonable; e.g., $M_z = 3.35$ eV Å^2, 9.25 eV Å^2, and 22.12 eV Å^2 for Bi_2Se_3, Bi_2Te_3, and Sb_2Te_3 [20]. Considering that M_z is usually less that 100 eV Å^2, it is safe to have the higher zero point of I_S. Therefore, we conclude that the zero point of I_S is only possible for either strong or weak topological insulator phases, in which the backscattering may be forbidden in the quantum limit.

Zeeman effect.—Above, we ignored the Zeeman effect, which we will show only quantitatively, but not qualitatively, changes the zero point of m and I_S. The Hamiltonian of the Zeeman part reads

$$H_z = \frac{\mu_B}{2}\begin{bmatrix} g_z^v B_z & g_p^v B_- & 0 & 0 \\ g_p^v B_+ & -g_z^v B_z & 0 & 0 \\ 0 & 0 & g_z^c B_z & g_p^c B_- \\ 0 & 0 & g_p^c B_+ & -g_z^c B_z \end{bmatrix}, \tag{7}$$

where μ_B is the Bohr magneton and $g_{z,p}^{v,c}$ are Landé g factors for valance or conduction bands along the z direction and in the x-y plane, respectively. With the Zeeman effect, the mass term is corrected to $m = M_0 + M_z k_z^2 + M_\perp(e/\hbar)B + B(g_z^c - g_z^v)\mu_B/4$, so the Zeeman effect is to correct $M_\perp$ to $\tilde{M}_\perp = M_\perp + (g_z^c - g_z^v)\mu_B\hbar/4e$. Figure 3 shows that the Zeeman effect does not change the physical picture in Fig. 2 much, but it shifts the zero point of I_S to lower magnetic fields.

Conductivity in the quantum limit.—Now we show how the resistivity is dictated by the backscattering (see details in Ref. [14]). Along the direction of the magnetic field, there is no Hall effect, so the resistivity is the inverse of the conductivity, i.e., $\rho_{zz} = 1/\sigma_{zz}$. In the quantum limit, the conductivity is contributed only by band 0+, and can be explicitly expressed in terms of the transport time $\tau_{k_F}^\pm$ at the two states $\pm k_F$ on the Fermi surface [10,12]

$$\sigma_{zz} = \frac{e^2}{h}\frac{\hbar v_F \Lambda}{2\pi\ell_B^2}\left(\frac{\tau_{k_F}^+}{\hbar} + \frac{\tau_{k_F}^-}{\hbar}\right), \tag{8}$$

where $-e$ is the electron charge, Λ is a value to correct the van Hove singularity at the band edge [10], and the Fermi velocity can be found as $\hbar v_F = \partial E_{0+}/\partial k_z|_{k_F}$. The transport time $\tau_{k_F}^\pm$ can be found as [12,29]

$$\frac{\hbar}{\tau_{k_F}^\pm} = 4\pi \sum_{k_x' k_z'} \langle |U_{0,0}^{k_z=\pm k_F, k_z'}|^2\rangle \frac{\Lambda\delta(k_z' \pm k_F)}{\hbar v_F}, \tag{9}$$

where $k_z' = \mp k_F$ for $k_z = \pm k_F$, so the transport time depicts the backscattering from k_F to $-k_F$, and vice versa. $U_{0,0}^{\pm k_F, \mp k_F}$ are the scattering matrix elements between the states k_F and $-k_F$, and $\langle \ldots \rangle$ means averaging over impurity configurations. Assume a general form of random

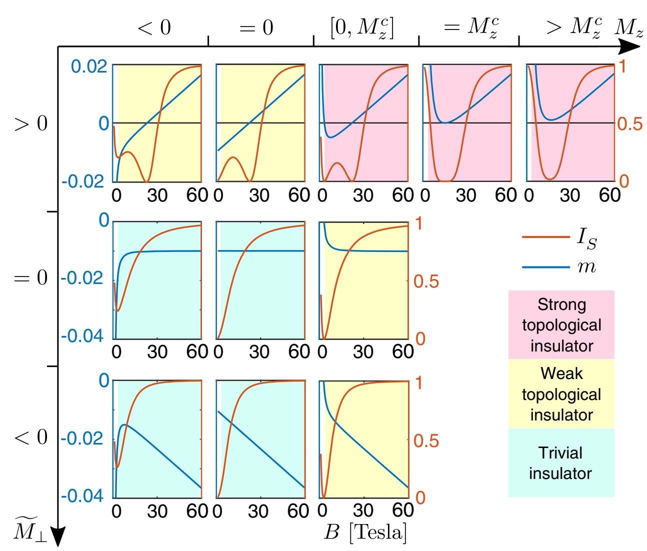

FIG. 3. The same as Fig. 2, but with the Zeeman effect, which shifts the zero point to a lower magnetic field. The parameters are the same as those in Fig. 2, except that $M_z = -27$, 0, 27, 205, 270 eV Å^2 from left to right; $g_z^c = 7.5$; and $g_z^v = -7.5$.

impurities $U(\mathbf{r}) = \sum_i U(\mathbf{r} - \mathbf{R}_i)$, where $\mathbf{R}_i$ are the positions of randomly distributed impurities and the function $U(\mathbf{r} - \mathbf{R}_i)$ depicts the impurity potential energy. Using the eigenstate in Eq. (3), the matrix element of the scattering between k_F and $-k_F$ can be expressed as

$$\langle |U_{0,0}^{k_z=k_F,k_z'=-k_F}|^2\rangle = I_S\langle |U_{0,0}|^2\rangle, \tag{10}$$

where I_S is the form factor in Eq. (5) and the rest depends on the specific form of $U(\mathbf{r})$ in real space. Equation (10) shows that no matter the form of the real-space part, the scattering matrix element and the inverse of the transport time always vanish when I_S vanishes. By understanding this and combining the above equations, the resitivity can be expressed as

$$\rho_{zz} = I_S/\sigma_0, \tag{11}$$

where σ_0 is the conductivity independent of the spinor inner product part. For different types of scattering potential, σ_0 takes different forms. But the form factor I_S in Eq. (11) dictates that a topological insulator always has a resistance dip, regardless of σ_0.

We can test the argument with a systematic calculation of σ_{zz}, in the presence of the Gaussian [12] and screened Coulomb [30,31] potentials, which are two common choices when describing the impurity scattering. For the Gaussian potential (see Ref. [14] for details),

$$\sigma_0 = \frac{e^2}{h}\frac{(\hbar v_F)^2(2d^2 + \ell_B^2)}{V_{\mathrm{imp}}\ell_B^2}e^{4d^2k_F^2}, \tag{12}$$

where d is the acting range of the Gaussian impurities, and V_{imp} measures the impurity density and scattering strength. As $d \to 0$, the conductivity reduces to $\sigma_0 = (e^2/h)(\hbar v_F)^2/V_{\mathrm{imp}}$. For the screened Coulomb potential (see Ref. [14] for details),

$$\sigma_0 = \frac{e^2}{h}\frac{\hbar v_F \Lambda \varepsilon}{\pi^2 n_{\mathrm{imp}} e^2 \ell_B^4}, \tag{13}$$

where ε is the dielectric constant and n_{imp} is the impurity density. Figure 4 and Fig. S2 of Ref. [14] show the resistivity in the presence of the Gaussian and screened Coulomb potentials. They both show clear dips in the resistivity for some weak topological phases ($M_z \le 0$ and $\tilde{M}_\perp > 0$ in row 1, columns 1 and 2) and strong topological insulator phases ($M_z \in [0, M_z^c]$ and $\tilde{M}_\perp > 0$ in row 1, column 3). More importantly, the positions of the minima on the B axis does not change for different potentials.

Spin-orbit scattering.—The spin-orbit scattering can improve the above picture and lead to a better fitting to the experiment. The spin configuration of our basis is $|\uparrow\rangle_1$, $|\downarrow\rangle_2$, $|\uparrow\rangle_3$, $|\downarrow\rangle_4$. We find that the off-diagonal spin-orbit scattering that couple 2 to 4 can change the result by lifting the exact forbidden backscattering (see Sec. S2B of Ref. [14]). This lifting can lead to a better fitting to a recent experiment on the topological insulator material $Pb_{1-x}Sn_xSe$ [13], which shows an unexpected suppression of the resistance in strong magnetic fields, as shown in Figs. 1(c) and 1(d). Specifically, in Fig. 1(d), we include the spin-orbit coupling in the screened Coulomb scattering potential. As a result, the resistivity is found to be

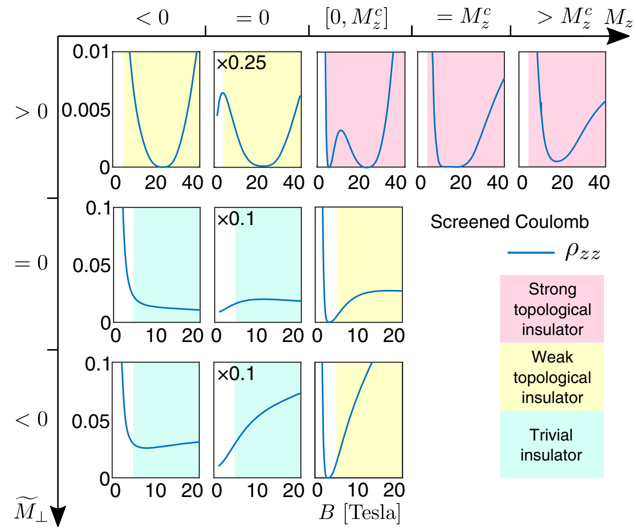

FIG. 4. The same as Fig. 3, but for the resistivity ρ_{zz} in the presence of the screened Coulomb scattering potential (in units of $2\pi^2\hbar n_{\mathrm{imp}}/e^2\varepsilon$). $C_z = 1.409$ eV Å^2. n_{imp} for the trivial insulator and topological insulator are $6.8\times10^{18}/\mathrm{cm}^3$ and $1.0\times10^{19}/\mathrm{cm}^3$, respectively. For $M_0 > 0$, the same results can be obtained by flipping $\tilde{M}_\perp$ and M_z accordingly. In the noncolored regions, the magnetic field is not strong enough to put all electrons into the lowest Landau bands.

$$\rho_{zz} = \frac{h\pi}{e^3 v_F^0 \Lambda B}\left(\alpha_1\frac{I_S}{B} + \alpha_2(1 - I_S)B^2\right), \tag{14}$$

where the α_1 term is due to the spin-independent scattering and diagonal spin-orbit scattering, and the α_2 term is due to the off-diagonal spin-orbit scattering. In experiments, they can serve as fitting parameters. By choosing proper α_1 and α_2, a −40% change is obtained at the dip of the resistance, consistent with the experiment, as shown in Figs. 1(c) and 1(d).

Experimental implications.—Although $Pb_{1-x}Sn_xSe$ is claimed to be a topological insulator, the interpretation in Ref. [13] adopted a theory for Weyl semimetal in delta scattering potentials [10,11], where the spinor wave function of the lowest Landau band takes the form

$$|0, k_x, k_z\rangle = \begin{bmatrix} 0 \\ |0\rangle \end{bmatrix} |k_x, k_z\rangle. \tag{15}$$

The spin part of the scattering matrix element is always 1, so a Weyl semimetal does not support the mechanism of the forbidden backscattering as the topological insulator does. In contrast, our theory gives a proper explanation and favors the experimentally observed resistance dip as a signature for weak topological insulators.

The resistance dip may not be observed in the Bi_2Se_3 family, because their large $M_0/\tilde{M}_\perp$ ratios require inaccessible magnetic fields for the dip (Table S1 of Ref. [14]). Our mechanism of forbidden backscattering is irrelevant to the details of impurities, and thus will be particularly useful for those controversial small-gap materials at the boundary between topological and normal insulators, such as the Ag_2Te [32] and $ZrTe_5$ [33,34] families, where controversies have built up over the years. In 2D, the quantum spin Hall phase may be probed by other approaches, such as interference effects [35], but this has nothing to do with our proposal in 3D.

This work was supported by the Guangdong Innovative and Entrepreneurial Research Team Program (Grant No. 2016ZT06D348), the National Basic Research Program of China (Grant No. 2015CB921102), the National Key R&D Program (Grant No. 2016YFA0301700), the National Natural Science Foundation of China (Grants No. 11534001 and No. 11574127), and the Science, Technology and Innovation Commission of Shenzhen Municipality (Grant No. ZDSYS20170303165926217).

*Corresponding author.
luhz@sustc.edu.cn

[1] M. Z. Hasan and C. L. Kane, Colloquium: Topological insulators, Rev. Mod. Phys. **82**, 3045 (2010).
[2] X.-L. Qi and S.-C. Zhang, Topological insulators and superconductors, Rev. Mod. Phys. **83**, 1057 (2011).
[3] S.-Q. Shen, *Topological Insulators*, 2nd ed. (Springer-Verlag, Berlin Heidelberg, 2017).
[4] R. Yu, W. Zhang, H.-J. Zhang, S.-C. Zhang, X. Dai, and Z. Fang, Quantized anomalous Hall effect in magnetic topological insulators, Science **329**, 61 (2010).
[5] C.-Z. Chang *et al.*, Experimental observation of the quantum anomalous Hall effect in a magnetic topological insulator, Science **340**, 167 (2013).
[6] L. Fu and C. L. Kane, Superconducting proximity effect and Majorana fermions at the surface of a topological insulator, Phys. Rev. Lett. **100**, 096407 (2008).
[7] A. R. Akhmerov, J. Nilsson, and C. W. J. Beenakker, Electrically detected interferometry of Majorana fermions in a topological insulator, Phys. Rev. Lett. **102**, 216404 (2009).
[8] M. König, S. Wiedmann, C. Brüne, A. Roth, H. Buhmann, L. W. Molenkamp, X.-L. Qi, and S.-C. Zhang, Quantum spin Hall insulator state in HgTe quantum wells, Science **318**, 766 (2007).
[9] B. Büttner *et al.*, Single valley Dirac fermions in zero-gap HgTe quantum wells, Nat. Phys. **7**, 418 (2011).
[10] H. Z. Lu, S. B. Zhang, and S. Q. Shen, High-field magnetoconductivity of topological semimetals with short-range potential, Phys. Rev. B **92**, 045203 (2015).
[11] P. Goswami, J. H. Pixley, and S. Das Sarma, Axial anomaly and longitudinal magnetoresistance of a generic three-dimensional metal, Phys. Rev. B **92**, 075205 (2015).
[12] S.-B. Zhang, H.-Z. Lu, and S.-Q. Shen, Linear magnetoconductivity in an intrinsic topological Weyl semimetal, New J. Phys. **18**, 053039 (2016).
[13] B. A. Assaf *et al.*, Negative longitudinal magnetoresistance from the anomalous $N = 0$ Landau level in topological materials, Phys. Rev. Lett. **119**, 106602 (2017).
[14] See Supplemental Material at http://link.aps.org/supplemental/10.1103/PhysRevLett.121.036602 for detailed calculations, which include Refs. [15–18].
[15] S. Hikami, A. I. Larkin, and Y. Nagaoka, Spin-orbit interaction and magnetoresistance in the two dimensional random system, Progr. Theor. Phys. **63**, 707 (1980).
[16] H.-Z. Lu, W. Yao, D. Xiao, and S.-Q. Shen, Intervalley scattering and localization behaviors of spin-valley coupled Dirac fermions, Phys. Rev. Lett. **110**, 016806 (2013).
[17] S. Datta, *Electronic Transport in Mesoscopic Systems* (Cambridge University Press, Cambridge, England, 1997).
[18] G. D. Mahan, *Many-Particle Physics* (Plenum Press, New York, 1990).
[19] H. Zhang, C.-X. Liu, X.-L. Qi, X. Dai, Z. Fang, and S.-C. Zhang, Topological insulators in Bi_2Se_3, Bi_2Te_3 and Sb_2Te_3 with a single Dirac cone on the surface, Nat. Phys. **5**, 438 (2009).
[20] I. A. Nechaev and E. E. Krasovskii, Relativistic $k \cdot p$ Hamiltonians for centrosymmetric topological insulators from *ab initio* wave functions, Phys. Rev. B **94**, 201410 (2016).
[21] H. Z. Lu, W. Y. Shan, W. Yao, Q. Niu, and S. Q. Shen, Massive Dirac fermions and spin physics in an ultrathin film of topological insulator, Phys. Rev. B **81**, 115407 (2010).
[22] W.-Y. Shan, H.-Z. Lu, and S.-Q. Shen, Effective continuous model for surface states and thin films of three-dimensional topological insulators, New J. Phys. **12**, 043048 (2010).
[23] Y. Zhang *et al.*, Crossover of the three-dimensional topological insulator Bi_2Se_3 to the two-dimensional limit, Nat. Phys. **6**, 584 (2010).
[24] X. Dai, Z. Z. Du, and H.-Z. Lu, Negative magnetoresistance without chiral anomaly in topological insulators, Phys. Rev. Lett. **119**, 166601 (2017).
[25] J. Wang *et al.*, Anomalous anisotropic magnetoresistance in topological insulator films, Nano Res. **5**, 739 (2012).
[26] H. T. He, H. C. Liu, B. K. Li, X. Guo, Z. J. Xu, M. H. Xie, and J. N. Wang, Disorder-induced linear magnetoresistance in (221) topological insulator Bi_2Se_3 films, Appl. Phys. Lett. **103**, 031606 (2013).
[27] S. Wiedmann *et al.*, Anisotropic and strong negative magnetoresistance in the three-dimensional topological insulator Bi_2Se_3, Phys. Rev. B **94**, 081302 (2016).
[28] L.-X. Wang, Y. Yan, L. Zhang, Z.-M. Liao, H.-C. Wu, and D.-P. Yu, Zeeman effect on surface electron transport in topological insulator Bi_2Se_3 nanoribbons, Nanoscale **7**, 16687 (2015).

[29] H.-Z. Lu, J. Shi, and S.-Q. Shen, Competition between weak localization and antilocalization in topological surface states, Phys. Rev. Lett. **107**, 076801 (2011).
[30] A. A. Abrikosov, Quantum magnetoresistance, Phys. Rev. B **58**, 2788 (1998).
[31] H. Bruus and K. Flensberg, *Many-Body Quantum Theory in Condensed Matter Physics: An Introduction* (Oxford Graduate Texts, New York, 2004).
[32] W. Zhang, R. Yu, W. Feng, Y. Yao, H. Weng, X. Dai, and Z. Fang, Topological aspect and quantum magnetoresistance of β-Ag_2Te, Phys. Rev. Lett. **106**, 156808 (2011).
[33] H. Weng, X. Dai, and Z. Fang, Transition-metal pentatelluride $ZrTe_5$ and $HfTe_5$: A paradigm for large-gap quantum spin Hall insulators, Phys. Rev. X **4**, 011002 (2014).
[34] Y. Liu *et al.*, Zeeman splitting and dynamical mass generation in Dirac semimetal $ZrTe_5$, Nat. Commun. **7**, 12516 (2016).
[35] A. Mani and C. Benjamin, Probing helicity and the topological origins of helicity via nonlocal Hanbury-Brown and Twiss correlations, Sci. Rep. **7**, 6954 (2017).